Frequency Domain Performance Analysis of Dynamic Decoupling Current Control in Buck and Boost Multiple Converters

Toshiyuki Fujita[1]*, Masahiro Mae[2], Hiroshi Fujimoto[1,2], Takayuki Miyajima[3], Yoshiki Yasuda[3], Akio Yamagiwa[3]
1 *Graduate School of Frontier Sciences*, *The University of Tokyo*, Chiba, Japan
2 *Graduate School of Engineering*, *The University of Tokyo*, Tokyo, Japan
3 *Technology and Innovation Center*, *DAIKIN INDUSTRIES, LTD.*, Osaka, Japan

***Abstract*—This paper presents a performance analysis of current control in a Multi-Input Multi-Output (MIMO) DC-DC converter system designed for residential energy management applications. The system comprises a boost converter and a high-voltage buck converter connected to a common DC link, representing typical configurations in home appliances and vehicle-to-everything systems. To investigate the impact of control bandwidth on system dynamics, both conventional and proposed Dynamic Decoupling Current Control (DDCC) methods are evaluated. The study employs transfer function modeling, sensitivity function, and complementary sensitivity function to assess stability under a typical operating condition. Experimental results confirm that simply increasing control bandwidth does not mitigate converter interaction. In contrast, the proposed DDCC method effectively suppresses interference, enhances stability, and shows a different low-frequency characteristic in the sensitivity function. These findings contribute to the design of robust and scalable control architectures for future energy management systems.**

***Index Terms*—Current control, DC-DC converter, Frequency analysis, Multi-input multi-output**

I. INTRODUCTION

The increasing integration of renewable energy sources, electric vehicles (EVs), and high-power household appliances has accelerated the development of advanced energy management systems (EMSs) for residential and commercial applications [1]–[3]. Recent work on hybrid-electric powertrains formulates EMS as an optimization problem over ignition scheduling and operating points, illustrating how multi-domain coordination (engine, inverter, storage) reshapes control objectives and constraints at the DC link level [4]. Another article investigates module- and interconnect-level parasitics that directly affect high-speed control performance, including S-parameter-based characterization of full-bridge power modules [5]. These findings are consistent with our observation that simply widening the current-control bandwidth does not guarantee decoupling; accurate plant representations must include parasitic dynamics and sensor/ADC limitations captured in the open-loop frequency response. The universal and modularization direction in power electronics continues to gain traction, as seen in the concept of Universal Smart Power Modules (USPM), which targets rapid system composition from building blocks and stresses fast feedback over shared links [6]. This research aligns with the EMS-integration goal in our study and further motivates rigorous MIMO stability tools (eigenvalue loci, MIMO Nyquist, and generalized Gershgorin bands) under model-plant mismatches.

EMSs often rely on multiple power converters—such as photovoltaic (PV) converters, battery chargers, and grid-tied inverters—connected to a common DC link [7]. This configuration enables flexible power flow control and efficient energy utilization, but also introduces complex dynamic interactions among converters that can compromise system stability and performance. Each converter is typically designed with its own current control loop. However, when multiple converters are connected to the same DC bus, their control loops become inherently coupled, forming a multi-input multi-output (MIMO) system. Conventional control strategies often neglect these interdependencies, treating the influence of other converters as disturbances or feedforward terms. While this simplification facilitates controller design, it can lead to degraded performance, especially under dynamic conditions such as load transients or source fluctuations. Moreover, the presence of constant power loads (CPLs), such as motor drives, further complicates the stability landscape [8]. CPLs exhibit negative incremental impedance characteristics, which can destabilize the DC bus voltage and induce oscillations [9]. These effects are exacerbated in MIMO converter systems, where the interaction between converters can amplify disturbances and reduce the effectiveness of traditional single-input single-output (SISO) control approaches.

To address these challenges, previous research has explored advanced modeling and Dynamic Decoupling Current Control (DDCC) techniques for MIMO power converter systems [10]. State-space averaging methods have been employed to derive small-signal models that capture the coupled dynamics of multiple converters. Frequency-domain analysis, including Bode and Nyquist diagrams, has been used to evaluate system stability and identify critical interaction pathways. In particular, the application of generalized Gershgorin bands in MIMO Nyquist

This work was partly supported by JSPS KAKENHI Grant Number 24K17256.

(C)2026IEEJ

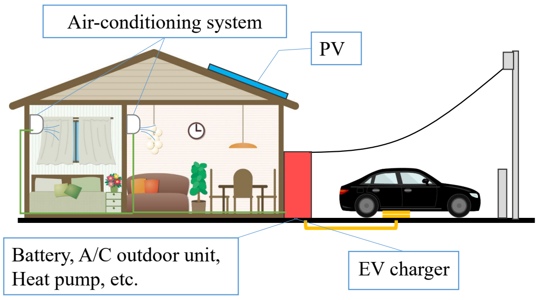

Fig. 1. Concept of the proposed system.

analysis has provided valuable insights into the robustness of control strategies under multi-axis interference.

Fig. 1 illustrates the envisioned EMS, which consolidates various high-power household devices—such as photovoltaic panels, battery storage units, air conditioning systems, grid-connected inverters, and electric vehicle chargers (each rated over 1 kW)—into a single, integrated control unit.

This paper studies a MIMO converter system—a configuration typical of residential EMS—complementary to a boost and a high-voltage buck converter connected to a shared DC link. The investigation includes the construction of a practical setup, the proposal of a DDCC method, and experimental validation. The core analysis focuses on the impact of high-speed current controllers on system dynamics, particularly how increased control bandwidth influences inter-converter interference and stability. To rigorously evaluate stability, the study employs frequency-domain techniques, including the transfer function, sensitivity function, and complementary sensitivity function. These analyses provide critical insights into the coupling effects between converters, demonstrating that increasing the control bandwidth alone does not achieve decoupling and clarifying the effectiveness of the proposed decoupling control.

II. Modeling and Control of MIMO Converter

A. Modeling of MIMO converters

Fig. 2 illustrates the system analyzed in this study, in which all converters are connected to a common DC link capacitor. The configuration consists of one buck converter, one boost converter, and an additional load referred to as "Other Load." To evaluate current controllability, the DC voltage v_{L} on the Other Load side is actively regulated. The parameters of the system are defined within Fig. 2.

Applying Kirchhoff's law to Fig. 2 yields:

$$\frac{\mathrm{d}}{\mathrm{d}t}x = f(x) = \begin{pmatrix} \frac{d_{\mathrm{PV}}}{L_{\mathrm{PV}}}V_{\mathrm{PV}} - \frac{r_{\mathrm{PV}}}{L_{\mathrm{PV}}}i_{\mathrm{PV}} - \frac{v_{\mathrm{L}}}{L_{\mathrm{PV}}} \\ -\frac{r_{\mathrm{B}}}{L_{\mathrm{B}}}i_{\mathrm{LB}} - \frac{(1-d_{\mathrm{B}})}{L_{\mathrm{B}}}v_{\mathrm{L}} + \frac{v_{\mathrm{L}}}{L_{\mathrm{B}}} \\ \frac{i_{\mathrm{PV}}}{C} + \frac{(1-d_{\mathrm{B}})}{C}i_{\mathrm{LB}} - \frac{i_e}{C} \end{pmatrix}. \quad (1)$$

$$\text{where} \quad x = \begin{pmatrix} i_{\mathrm{PV}} & i_{\mathrm{LB}} & v_{\mathrm{L}}. \end{pmatrix}^{\mathsf{T}}$$

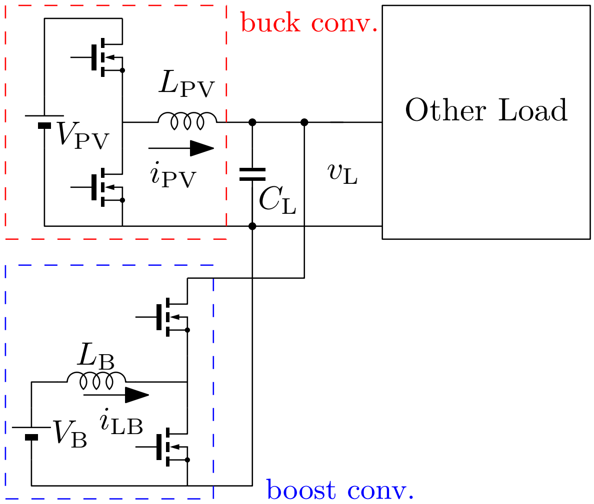

Fig. 2. Circuit configuration of the analyzed system, in which all converters are connected to a common DC link capacitor C_{L}. The system consists of one buck converter, one boost converter, and an additional load ("Other Load").

Fig. 3 illustrates the conventional control structure of the system, where the plant P corresponds to the circuit shown in Fig. 2. The current controllers C_{PV} and C_{B} are implemented as proportional-integral (PI) controllers, designed under the assumption that the plant behaves as a first-order system. The gains of the controllers are discussed in section II-B. Linearizing Eq. (1) around the steady-state operating point yields the small-signal state-space representation shown in Eqs. (2) and (3), from which the transfer function relating the input perturbations Δu_{C} to the output responses Δy is derived, where $d'_{\mathrm{B}} = 1 - d_{\mathrm{B}}$;

$$\frac{d}{dt}\Delta x = A_{\mathrm{C}}\Delta x + B_{\mathrm{C}}\Delta u_{\mathrm{C}}, \quad (2)$$

$$\Delta y = C\Delta x, \quad (3)$$

where

$$\Delta u^{\mathrm{C}} = \begin{pmatrix} \Delta v_{\mathrm{PV}}^{\mathrm{C}} & \Delta v_{\mathrm{B}}^{\mathrm{C}} \end{pmatrix}^{\mathsf{T}} = \begin{pmatrix} \Delta d_{\mathrm{PV}}V_{\mathrm{PV}} & -\Delta d'_{\mathrm{B}}V_{\mathrm{L}} \end{pmatrix}^{\mathsf{T}},$$

$$A_{\mathrm{C}} = \frac{\partial f}{\partial x_k} = \begin{pmatrix} -\frac{r_{\mathrm{PV}}}{L_{\mathrm{PV}}} & 0 & -\frac{1}{L_{\mathrm{PV}}} \\ 0 & -\frac{r_{\mathrm{B}}}{L_{\mathrm{B}}} & -\frac{D'_{\mathrm{B}}}{L_{\mathrm{B}}} \\ \frac{1}{C} & \frac{D'_{\mathrm{B}}}{C} & 0 \end{pmatrix},$$

$$B_{\mathrm{C}} = \frac{\partial f}{\partial u_k} = \begin{pmatrix} \frac{1}{L_{\mathrm{PV}}} & 0 \\ 0 & \frac{1}{L_{\mathrm{B}}} \\ 0 & -\frac{I_{\mathrm{LB}}}{CV_{\mathrm{L}}} \end{pmatrix},$$

$$C = \begin{pmatrix} 1 & 0 & 0 \\ 0 & 1 & 0 \\ 0 & 0 & 0 \end{pmatrix}.$$

Fig. 4 illustrates the proposed DDCC structure of the system. Controllers are the same as the conventional controllers. DDCC method achieves the decoupling using Δv_{L} to internal

(C)2026IEEJ

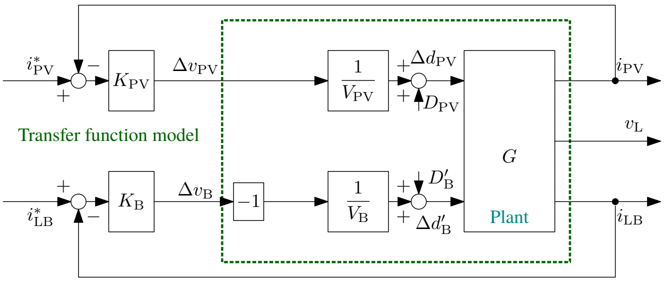

Fig. 3. Block diagram of conventional control

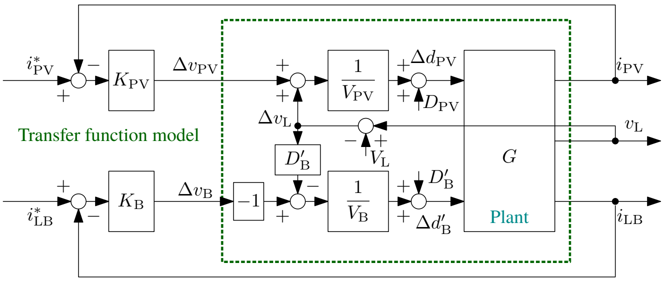

Fig. 4. Block diagram of proposed Dynamic Decoupling Current Control

inputs. The decoupled state-space equation is calculated using Eq. (2) and the newly defined inputs u_{D};

$$
\begin{aligned}
\frac{d}{dt}\Delta x &= A_{\mathrm{D}}\Delta x + B_{\mathrm{D}}\Delta u_{\mathrm{D}}, &(4)\\
\Delta y &= C\Delta x, &(5)\\
\text{where}\quad \Delta u^{\mathrm{D}} &= \begin{pmatrix}\Delta v_{\mathrm{PV}}^{\mathrm{D}} & \Delta v_{\mathrm{B}}^{\mathrm{D}}\end{pmatrix}^{\mathsf{T}}\\
&= \begin{pmatrix}\Delta v_{\mathrm{PV}}^{\mathrm{C}} + \Delta v_{\mathrm{L}} & -\Delta v_{\mathrm{B}}^{\mathrm{C}} + D_{\mathrm{B}}'\Delta v_{\mathrm{L}}\end{pmatrix}^{\mathsf{T}},\\
A_{\mathrm{D}} &= \begin{pmatrix} -\frac{r_{\mathrm{PV}}}{L_{\mathrm{PV}}} & 0 & 0\\ 0 & -\frac{r_{\mathrm{B}}}{L_{\mathrm{B}}} & 0\\ \frac{1}{C} & \frac{D_{\mathrm{B}}'}{C} & -\frac{D_{\mathrm{B}}' I_{\mathrm{LB}}}{C V_{\mathrm{L}}}\end{pmatrix},\\
B_{\mathrm{D}} &= \begin{pmatrix} \frac{1}{L_{\mathrm{PV}}} & 0\\ 0 & \frac{1}{L_{\mathrm{B}}}\\ 0 & -\frac{I_{\mathrm{LB}}}{C V_{\mathrm{L}}}\end{pmatrix}.
\end{aligned}
$$

These two state-space equations G_{C} and G_{D} are calculated to the transfer functions below;

$$
\begin{aligned}
G_{\mathrm{C}} &= \frac{\Delta y}{\Delta u_{\mathrm{C}}} = C(sI - \Delta A_{\mathrm{C}})^{-1}\Delta B_{\mathrm{C}} &(6)\\
&= \begin{pmatrix} \dfrac{\left(s + \frac{r_{\mathrm{B}}}{L_{\mathrm{B}}}\right)s + \frac{D_{\mathrm{B}}'^2}{C L_{\mathrm{B}}}}{L_{\mathrm{PV}}\Phi} & \dfrac{\frac{I_{\mathrm{LB}}}{V_{\mathrm{L}}}\left(s + \frac{r_{\mathrm{B}}}{L_{\mathrm{B}}}\right) - \frac{D_{\mathrm{B}}'}{L_{\mathrm{B}}}}{C L_{\mathrm{B}}\Phi}\\ -\dfrac{D_{\mathrm{B}}}{C L_{\mathrm{PV}} L_{\mathrm{B}}\Phi} & \dfrac{\left(s + \frac{r_{\mathrm{PV}}}{L_{\mathrm{PV}}}\right)\left(s + \frac{D_{\mathrm{B}}' I_{\mathrm{LB}}}{C V_{\mathrm{L}}}\right)}{L_{\mathrm{B}}\Phi}\end{pmatrix},
\end{aligned}
$$

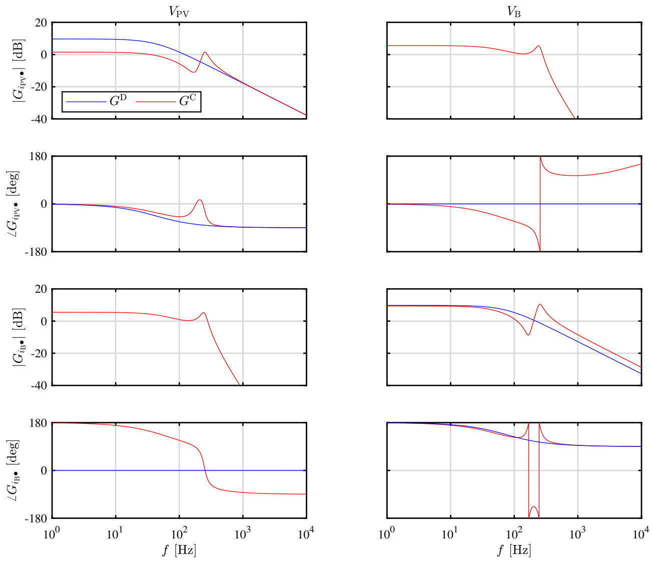

Fig. 5. Frequency response data of the conventional and proposed models G^{C} and G^{D}.

TABLE I
EXPERIMENTAL PARAMETERS OF THE STEP RESPONSES.

Parameter	Value	Parameter	Value
V_{PV}	200 V	V_{B}	100 V
L_{PV}	404 μH	r_{PV}	0.422 Ω
L_{B}	447 μ H	r_{B}	0.253 Ω
ω_{PV}	960 Hz	ω_{B}	960 Hz

TABLE II
INITIAL CONDITION OF THE COMMAND VALUE AND STEADY-STATE OPERATIONG POINT

Parameter	Value	Parameter	Value
I_{PV}^*	4 A	I_{LB}^*	5 A
I_e^*	0 A	V_{link}^*	160 V

$$
\begin{aligned}
\Phi &= s^3 + \left(\tfrac{r_{\mathrm{PV}}}{L_{\mathrm{PV}}} + \tfrac{r_{\mathrm{B}}}{L_{\mathrm{B}}}\right)s^2\\
&\quad + \left(\tfrac{r_{\mathrm{PV}} r_{\mathrm{B}}}{L_{\mathrm{PV}} L_{\mathrm{B}}} + \tfrac{1}{C_L \mathrm{PV}} + \tfrac{D_{\mathrm{B}}'^2}{C L_{\mathrm{B}}}\right)s + \frac{r_{\mathrm{B}} + r_{\mathrm{PV}} D_{\mathrm{B}}'^2}{C L_{\mathrm{PV}} L_{\mathrm{B}}},\\
G_{\mathrm{D}} &= \frac{\Delta y}{\Delta u_{\mathrm{D}}} = C(sI - \Delta A_{\mathrm{D}})^{-1}\Delta B_{\mathrm{D}} &(7)\\
&= \begin{pmatrix} \dfrac{1}{L_{\mathrm{PV}} s + r_{\mathrm{PV}}} & 0\\ 0 & \dfrac{1}{L_{\mathrm{B}} s + r_{\mathrm{B}}}\end{pmatrix}.
\end{aligned}
$$

Fig. 5 shows the experimental frequency response data of the conventional and decoupled methods. The system parameters are listed in Table I, II.

Fig. 6 presents the Relative Gain Array (RGA) for the conventional and decoupled methods, based on both model-based calculations and experimental results [11]. The system parameters used in this analysis are detailed in Table I. As a practical tool for assessing control loop interaction, the RGA

(C)2026IEEJ

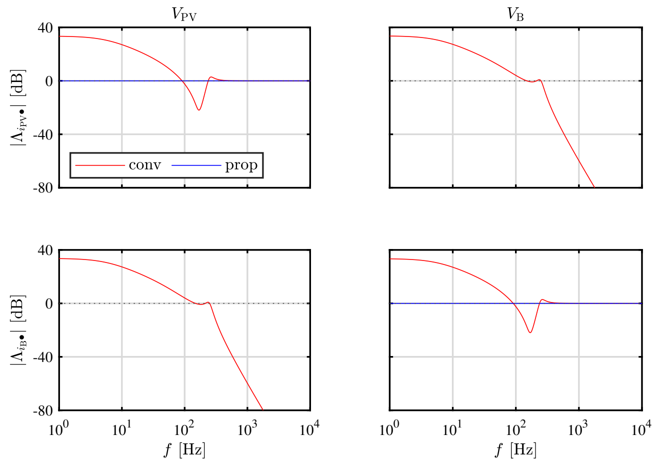

Fig. 6. Relative Gain Array of conventional and proposed transfer functions G^{C} and G^{D}.

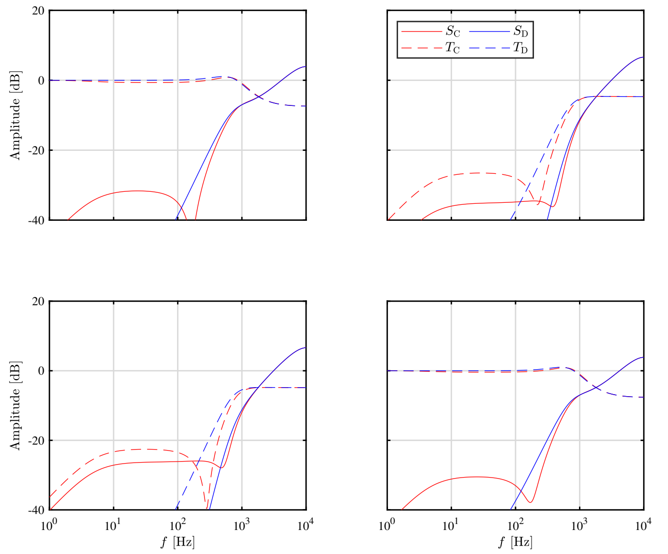

Fig. 7. Sensitivity and complementary sensitivity functions with the conventional and proposed DDCC method with a 960 Hz bandwidth controller when $I_e = 0$.

Λ is calculated as:

$$\Lambda = G \circ (G^{-1})^{\mathsf{T}}, \tag{8}$$
$$\Lambda_{ij} = \lambda_{ij} = [G]_{ij}[G^{-1}]_{ji}.$$

"$\circ$" denotes Hadamard product which means element-by-element multiplication of the matrix. RGA is independent of input and output scaling. Note that dominant input and output pairs have 0 dB of RGA, and other pairs are very small; in other words, they are decoupled. Λ_{11} and Λ_{22} of the proposed DDCC method are 0dB, and the off-diagonal terms are not displayed since the interrelations are extremely low in the all-frequency range. The anti-resonant frequency of the conventional method in the diagonal terms is around 150 Hz. The gain of the off-diagonal terms below 200 Hz exceeds 0 dB, so the influence of the off-diagonal terms becomes stronger in the low frequency range.

B. Current Controller design of the system

The conventional and proposed PI gains of the current controller K are determined using the pole placement method of a SISO converter model. The proposed decoupled PI gains are the same as a SISO converter model shown in Eq. (7).

$$K = \begin{pmatrix} K_{\mathrm{PV}} & 0 \\ 0 & K_{\mathrm{B}} \end{pmatrix}. \tag{9}$$

where

$$K_{\mathrm{PV}} = 2\omega_{\mathrm{PV}}L_{\mathrm{PV}} - r_{\mathrm{PV}} + \frac{\omega_{\mathrm{PV}}^2 L_{\mathrm{PV}}}{s},$$
$$K_{\mathrm{B}} = 2\omega_{\mathrm{B}}L_{\mathrm{B}} - r_{\mathrm{B}} + \frac{\omega_{\mathrm{B}}^2 L_{\mathrm{B}}}{s}.$$

ω_{PV} and ω_{B} are angular frequency of the pole. The pole placement method is more stable than the pole-zero cancellation even when there is a modeling error in the control plant. For analytical convenience, the pole frequencies of the PV and battery converters, denoted as ω_{PV} and ω_{B}, respectively, are assumed to be equal.

C. Frequency Analysis using Sensitivity and Complementary Sensitivity Functions

Sensitivity function S_i and complementary sensitivity function T_i are defined below;

$$S_i = (I + G_iK)^{-1} \tag{10}$$
$$T_i = G_iK(I + G_iK)^{-1} \tag{11}$$

where i denotes PV or B.

The sensitivity function S indicates the transfer characteristics from a disturbance to the output, thereby showing the disturbance suppression performance. A lower S value signifies better disturbance suppression. The complementary sensitivity function T indicates the transfer characteristics from output noise to the output, which represents the system's noise resistance. The closer T is to 1, which means 0dB, the better the command value tracking performance.

Fig. 7 shows the sensitivity and complementary sensitivity functions with the conventional and proposed DDCC method. S and T show consistency between the conventional and proposed methods above 1 kHz. However, the low-frequency characteristics differ. In the conventional method, the diagonal terms of S_{C11} and S_{C22} maintain a gain of approximately -30dB. In contrast, the off-diagonal terms, S_{C12} and S_{C21}, retain gains of approximately -35dB and -27dB, respectively. Furthermore, in the conventional method, the off-diagonal terms T_{C12} and T_{C21}, with gains of -27dB and -25dB, also remain significantly large. The response of these relatively high-gain off-diagonal terms overlaps with the diagonal terms, acting as disturbances. Specifically, T_{C12} has a higher gain than S_{C11} and might cause divergence due to a limit cycle. The frequency at which S_{C11} reaches its minimum value is approximately 150 Hz.

(C)2026IEEJ

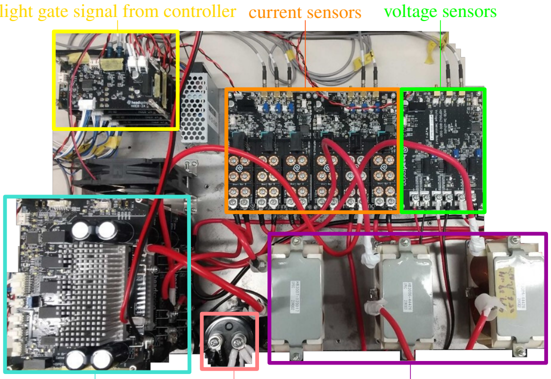

Fig. 8. Overview photograph of the experimental setup.

III. Experimental Step Response

Fig. 8 describes the experimental setup for the experiment. Circuit configurations are shown in Fig. 2. The parameters of the system are listed in Table I. The steady-state operating point is set to approximately half of the rated current. And the DC link voltage V_{L} is set to a value slightly larger than the maximum amplitude, taking into account the connection to a 100 V AC grid.

Figs. 9 present the current step responses of the system. The DC link voltage v_{L} is controlled by Other Load, the bandwidth of the voltage controller ω_{V} is 30 Hz. The convergence speed of the DC link voltage is the same between the conventional and DDCC methods because the voltage controller remains unchanged. After the step, saturation of the duty d_{PV} was observed for both the conventional and the proposed DDCC method. However, the conventional method exhibits the current oscillations due to d_{PV}. In contrast, the proposed method of d_{PV} hits the maximum limit immediately after the step, but then converges after 30 ms. The oscillation frequency of the conventional control and proposed DDCC current i_{LB} envelopes are 150 and 480 Hz, respectively. Also, the oscillations of the current i_{PV} are 150 and 100 Hz. The current oscillation frequency of the conventional method aligns with the experimental results and sensitivity analysis discussed in Section II-C.

IV. Conclusion

This paper analyzes a MIMO converter system, typical of residential EMS, consisting of a boost and a high-voltage buck converter connected to a shared DC link. The research included constructing a practical setup, proposing the DDCC method, and conducting experimental validation. The core analysis focused on how increased control bandwidth of high-speed current controllers influences inter-converter interference and stability. To evaluate stability rigorously, the study used frequency-domain techniques, including the transfer function, sensitivity function (S), and complementary sensitivity function (T). The analyses showed that merely

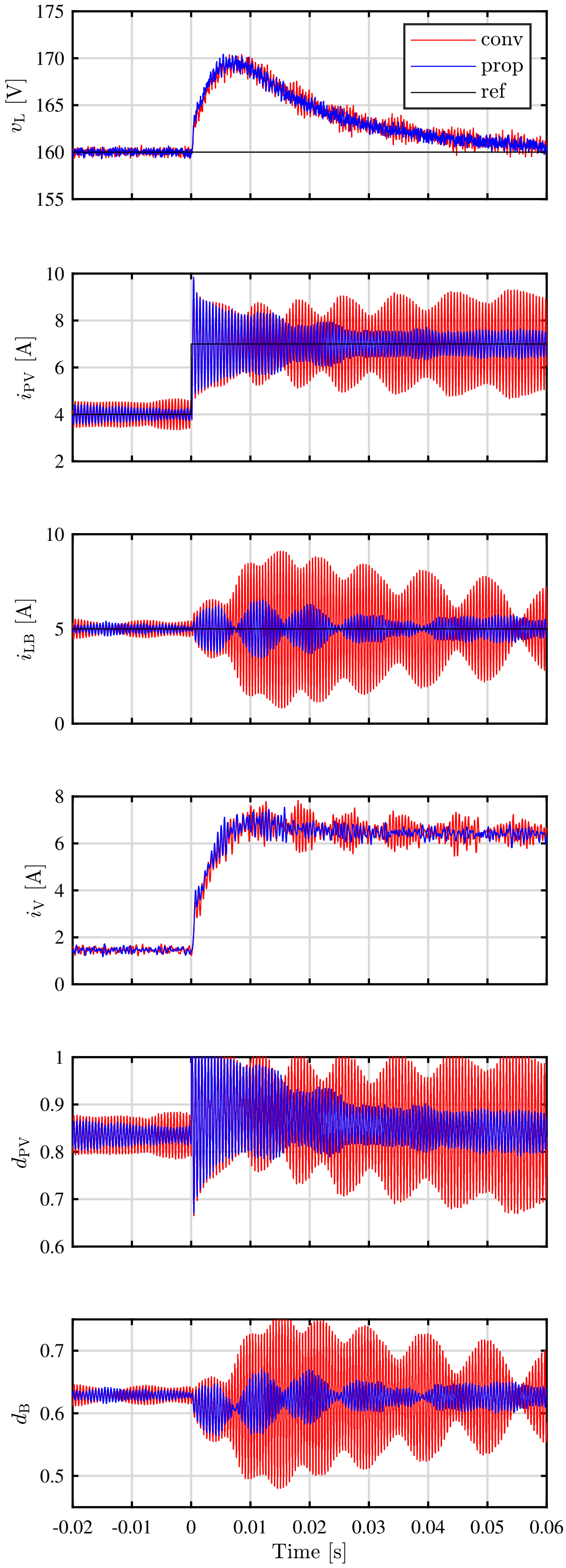

Fig. 9. Step responses of current control with a 960 Hz bandwidth when $I_e = 0$.

(C)2026IEEJ

increasing the control bandwidth does not achieve decoupling. Specifically, conventional control exhibits oscillations and limit cycles in current, with the high-gain off-diagonal terms of T acting as disturbances. The oscillation frequency observed in experiments at 150 Hz matches the frequency where $S_{\mathrm{C}11}$ is minimum. The research clarifies the effectiveness of the proposed decoupling control in suppressing interference and stabilizing the system.

REFERENCES

[1] N. Yang, G. Xu, Z. Fei, Z. Li, L. Du, J. M. Guerrero, Y. Huang, J. Yan, C. Xing, and Z. Li, "Two-stage coordinated robust planning of multi-energy ship microgrids considering thermal inertia and ship navigation," *IEEE Transactions on Smart Grid*, vol. 16, no. 2, pp. 1100–1111, 2025.

[2] B. Daftary Besheli, F. Cecati, S. Pugliese, M. L. Fellow, J. K. M. Becker, and M. Paolone, "Stability analysis and hil validation of pv park voltage control considering communication delays," *IEEE Open Journal of Power Electronics*, vol. 6, pp. 931–946, 2025.

[3] Y. Mitsugi and J. Baba, "Phaser-based transfer function analysis of power synchronization control instability for a grid forming inverter in a stiff grid," *IEEE Access*, vol. 11, pp. 42 146–42 159, 2023.

[4] W. Cao, R. Goto, T. Yuno, T. Kawabe, and M. Mukai, "Energy management method optimizing engine ignition on/off timing and operating points of powertrain components for series hybrid electric vehicle," *IEEJ Journal of Industry Applications*, vol. 14, no. 3, pp. 366–375, 2025.

[5] Deepankar, T. Ibuchi, and T. Funaki, "Parasitic inductance characterization of full-bridge power module based on s-parameter measurements," *IEEJ Journal of Industry Applications*, vol. 14, no. 3, pp. 477–483, 2025.

[6] H. Watanabe, K. Yamanokuchi, Y. Ikeda, Y. Takahashi, and J.-i. Itoh, "Universal smart power module (uspm) for carbon neutral society," *IEEE Transactions on Industry Applications*, vol. 60, no. 2, pp. 3411–3417, 2024.

[7] S. Gaurav, S. Pugliese, M. Langwasser, C. Kumar, and M. Liserre, "Power control in andronov-hopf virtual oscillator converters for st-based lv distribution systems," *IEEE Transactions on Industrial Electronics*, vol. 72, no. 9, pp. 9239–9249, 2025.

[8] J. Chai, Z. Xu, M. Wang, and X. Lyu, "Information-exchange-reduced distributed fixed-time secondary control for dc microgrid with enhanced stability," *IEEE Transactions on Industry Applications*, vol. 61, no. 5, pp. 8064–8079, 2025.

[9] A. Emadi, A. Khaligh, C. Rivetta, and G. Williamson, "Constant power loads and negative impedance instability in automotive systems: definition, modeling, stability, and control of power electronic converters and motor drives," *IEEE Transactions on Vehicular Technology*, vol. 55, no. 4, pp. 1112–1125, 2006.

[10] T. Fujita, M. Mae, H. Fujimoto, M. Nakagawa, Y. Yasuda, and A. Yamagiwa, "Dynamic decoupling current control of boost and buck multiple converters," *IEEE Transactions on Power Electronics*, pp. 1–11, 2025.

[11] S. Skogestad and I. Postlethwaite, *Multivariable Feedback Control*, 2nd ed. John Wiley and Sons Ltd., 2005.

(C)2026IEEJ